Journal of Materials Chemistry A

Accepted Manuscript

ROYAL SOCIETY OF CHEMISTRY

www.rsc.org/materialsA

Fiber-shaped Perovskite Solar Cells With 5.3% Efficiency

Hsienwei Hu[a], Kai Yan[a], Ming Peng[a], Xiao Yu[a], Si Chen[a], Buxin Chen[a], Bin Dong[a], Xue Gao[a] and Dechun Zou[*ab]

[a]Beijing National Laboratory for Molecular Sciences, Key Laboratory of Polymer Chemistry and Physics of Ministry of Education, Center for Soft Matter Science and Engineering, College of Chemistry and Molecular Engineering, Peking University, Beijing 100871, China. E-mail: dczou@pku.edu.cn; Fax: +86-10-6275-9799; Tel: +86-10-6275-9799

[b]Beijing Engineering Research Center for Active Matrix Display, Peking University, Beijing 100871, China

Abstract

Nowadays, there is an increasing interest in solid solar cells based on organolead trihalides, which have achieved certified efficiency of 20.1%. The success in perovskite solar cells extended the knowledge of perovskite materials and inspired their research for special solar architectures. Fiber-shaped solar cells are a kind of photovoltaic devices fabricated on one-dimensional conductive substrates, which could be potential candidates for wearable/portable electronics. In this work, we integrate the structure of Ti/c-TiO_2/meso-TiO_2/perovskite/Spiro-OMeTAD/Au into the fiber format. The fiber-shaped perovskite solar cells achieved PCE of 5.3% under AM 1.5 illumination and apparent efficiency of 8.4% in the diffuse model. The device design requires no transparent conductive oxides and thin film of gold nanoparticles was employed as the semitransparent top electrode. All the processes for device fabrication are easy to handle and energy-saving. The fiber devices exhibited high

reproducibility, which could open new doors toward efficient solid fiber shaped photovoltaic cells.

Keywords: Perovskite solar cell, fiber-shaped solar cell, electric heating, gold nanoparticles

Introduction

Perovskite solar cells (PSCs) based on organic–inorganic hybrid halide perovskite materials (e.g., $CH_3NH_3PbX_3$, X = Cl, Br, I) have attracted attention from both academe and industry because of their potential high performance and easy preparation. [1,2] Perovskite materials have exhibited excellent light harvesting, high charge-carrier mobility, long exciton diffusion length, long excited carrier lifetime, and small exciton binding energy.[3,4,5,6] PSCs functional layers can also be processed with solution or gas sources at rather low temperature.[7,8,9] PSCs have developed rapidly in the last three years, and achieved a certified power conversion efficiency (PCE) of 20.1%.[10] The development of PSCs was claimed to begin the new era of photovoltaics and created new opportunities for future solar designs.[11,12]

As a solar architecture offering special power supply, fiber-shaped solar cells are photovoltaic solar cells in the linear shape, which could harvest solar energy from 3D space due to their symmetrical structure and could be potential flexible power sources because of their adjustable aspect ratio.[13] Recent flexible fiber shaped solar cells have the potential to be woven into clothes and can contribute to wearable and electronic textiles of the next generation.[14] Fiber dye-sensitized solar cells can achieve

efficiencies of up to 8%[15,16], but the volatile electrolyte requires additional package. Solid fiber solar cells could avoid the problem, but both organic and inorganic fiber photovoltaic cells exhibited relatively lower efficiencies (0.5%-3.9%).[17, 18,19] Efficient PSCs may pave the way for potential breakthroughs for fiber photovoltaic devices. One of the main concerns of solid fiber devices is the top electrode materials that requires excellent balance between the transparence for enough light harvesting and the conductivity for good charge collection. In the early attempts, Peng *et al.* reported fiber-shaped perovskite solar cells with multi-walled carbon nanotube sheets as the top electrode and obtained a maximum PCE of 3.3%[20], which opened a door for future improvement. But the non-metal material would suffer from increased resistance especially in large-size devices. Minoh Lee *et al.* employed silver nanowires as the top electrode in with spray-deposition, and their device exhibited a PCE of 3.85%[21], but the deposition process of the silver nanowires may do harm to the perovskite film and the detrimental effect of silver nanowires and hole-transport material lead to S-shaped J-V curves. Considering the high performance of traditional perovskite solar cells, fiber-shaped perovskite solar cells (FPSCs) still have much room for improvement. Further, high-quality film is the basic requirement toward efficient FPSCs. The fill factors of solid fiber solar cells have turned out to be a limiting factor probably because unpreferable film morphology and interface defects on the curved substrate lead to limited photoelectron generation and charge transport. Also, the spin-coating process involved in typical preparation may not be practical for wire substrates. Thus, attempts in materials selection, interface engineering, structure

designs, and preparation process will further enhance the basic performance of fiber-shaped perovskite solar cells and lay the foundation for future modularization.

In this report, we integrated typical perovskite solar cells into fiber-shaped devices and achieved a PCE of 5.35%. To the best of our knowledge, the device performance is among the best results for solid fiber solar cells. $CH_3NH_3PbI_{3-x}Cl_x$ was employed as a functional layer via simple dip-coating, and the thin film of gold nanoparticles produced via magnetron sputtering was used as semitransparent top electrode for the fiber perovskite solar cells. The effects of electric heating, thickness of the mesoporous TiO_2 layer, and morphology of the perovskite layer were studied. The preparation is easy to handle and the device reproducibility is promising. The results of our work may open new doors toward the development of efficient fiber solid solar cells.

Results and Discussion

Referencing the structure of traditional PSCs, we designed novel FPSCs with the structure of Ti/ c-TiO_2/meso-TiO_2/perovskite/Spiro-OMeTAD/Au as shown in Figure 1a. The compact TiO_2 layer were prepared in situ on a titanium wire via electric heating followed by dip-coating with TiO_2 colloids as mesoporous layer. The $CH_3NH_3PbI_{3-x}Cl_x$ perovskite layer and Spiro-OMeTAD hole-transport layer fabrication were solution-processed. The thin film of gold nanoparticles produced via magnetron sputtering was employed as semi-transparent electrode for light harvesting and charge collection. This fiber is highly symmetrical and can harvest solar energy

from 3D space. As shown in Figure 1b, each functional layer could be observed in the cross-sectional of a shedding layer. A flexible gold wire (25 μm) was twisted around the fiber as the lead electrode (as shown in Figure 1c). The FPSC is one-dimensional in the macro perspective, but actually has a three-dimensional microscopic structure. The methods and details for preparing the functional layers are presented in the following.

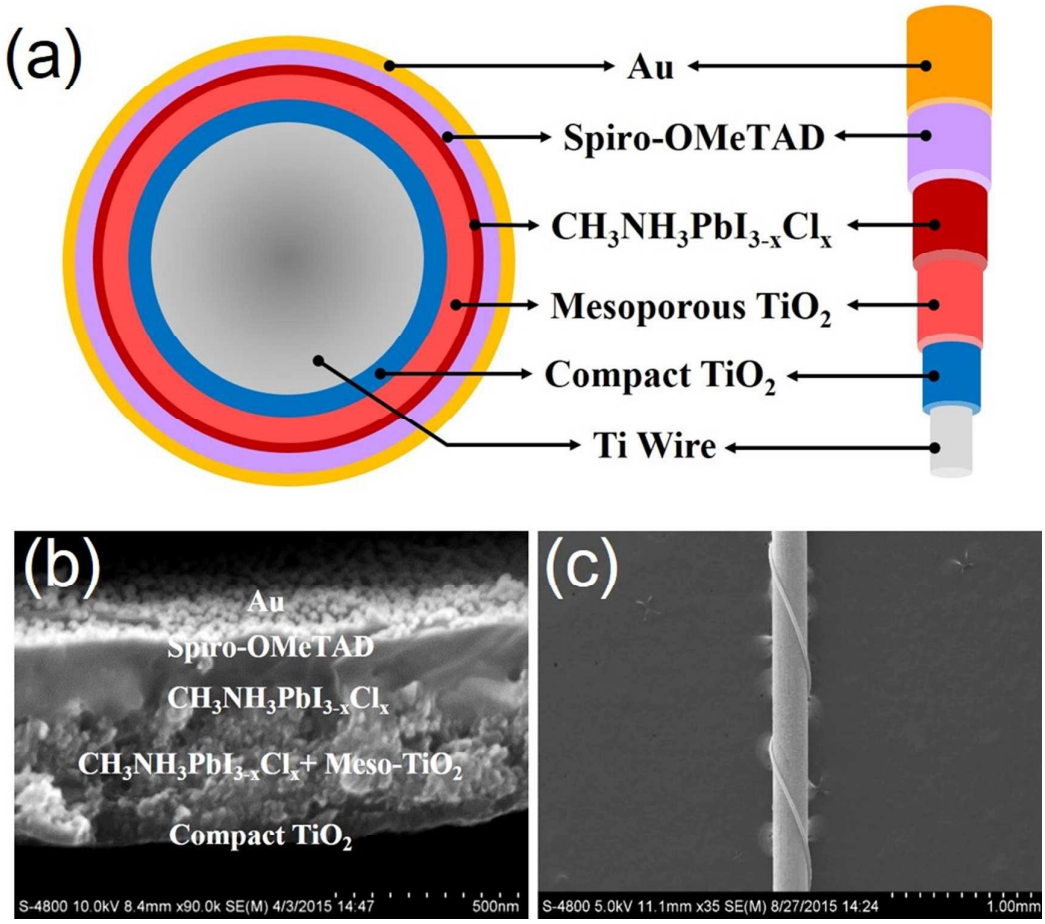

Figure 1. (a) Schematic of the fiber-shaped perovskite solar cell (FPSC) structure. (b) SEM cross-sectional image of the FPSC. (c) Image of typical FPSC.

Since the substrate surface is highly curved and total thickness of the perovskite

solar cell device is less than 1 μm, a substrate with smooth surface is required to avoid potential defects. Otherwise the film will become very uneven, which would aggravate charge recombination. For substrate pretreatment, mechanical polishing was used to smoothen the substrate surface, and a significantly improved surface smoothness could be observed after pretreatment (Figure S1). With pretreatment, the follow-up film quality could be guaranteed and lay the foundation toward high-efficiency FPSCs.

On this basis, a high quality compact layer is necessary to avoid short-circuit.[22] The solution method is the common method used in compact layer preparation. Titanate isopropyl acidic alcohol solution is used to coat the fiber, and the fiber substrate is annealed at 400 °C to generate a TiO_2 compact layer.[23] However, the compact layer of the fiber-shaped solar cells produced by the solution method cracks easily after annealing because the fiber surface is highly curved (Figure 2a). To improving the quality of compact layer, we use electric heating to generate a compact TiO_2 layer in situ by oxidation reaction between the Ti wire and oxygen in the air. The film generated using this method is highly compact and complete (Figure 2b) and can prevent the device from short-circuit. The FPSC without electric heating obtained V_{oc} of 0.624 V, J_{sc} of 12.46 mA/cm^2, FF of 0.40, and PCE of 3.09%. The FPSC with 2 min of electric heating achieved V_{oc} of 0.60 V, J_{sc} of 12.30 mA/cm^2, FF of 0.60, and PCE of 4.5%. And obvious FF improvement from 0.40 to 0.60 was observed because the compact TiO_2 layer could improve the interface charge transfer and match the energy level of perovskite layer. However, the thickness of the compact layer

increases with increasing processing time, resulting in the large series resistance. Obvious decrease of the short-circuit current (Jsc) density decreases from 12.3 to 3.94 mA/cm^2 is observed as the heat time increased from 2 min to 20 min (as shown in Figure 2c).

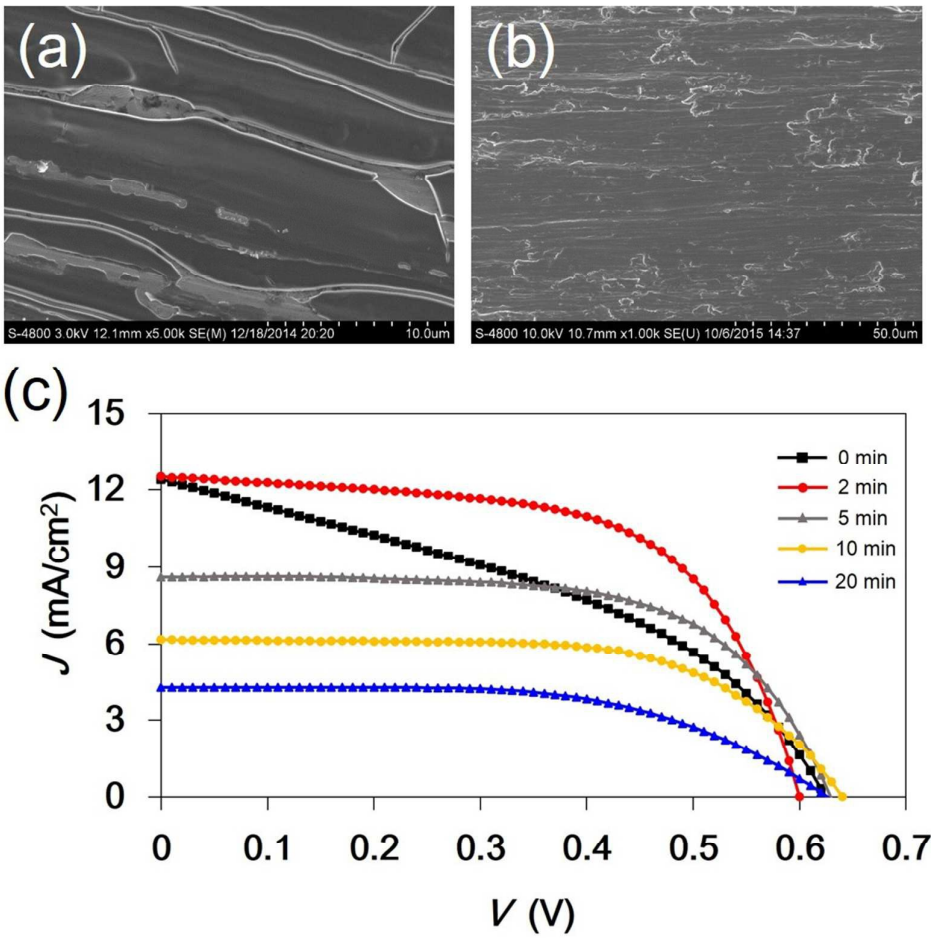

Figure 2. Compact layer prepared (a) by the solution method and (b) by electric heating. (c) J–V curves of FPSCs with various electric heating durations.

However, the smooth compact layer with high curvature is difficult to absorb perovskite materials. Thus, a mesoporous TiO_2 layer was employed to increase the loading amount of perovskite functional materials. To generate a uniform,

high-quality, and stable mesoporous TiO_2 layer, a half-automation coating setup was used. TiO_2 colloid was coated onto the fiber substrate with a current of 0.7 A for heating, which will make the TiO_2 porous layer smoother. The mesoporous TiO_2 layer was annealed by electric heating instead of air heating. It is worth noting that, the autologous heating process is more uniform and energy-saving than air heating, which could be applied to other optical electronics. The mesoporous TiO_2 layer as prepared on the substrate was very uniform and smooth (Figures 3a and 3b), and we find the process is highly repeatable. The thickness of the mesoporous TiO_2 layer is an important factor to achieve high-efficiency FPSCs. Mesoporous TiO_2 layers with different thicknesses were applied (including no mesoporous TiO_2 layer) to FPSCs, and the efficiencies of the resultant devices were measured. Figure 3c demonstrates that the optimized thickness of the mesoporous TiO_2 layer is 300 nm, with V_{oc} of 0.62 V, J_{sc} of 11.49 mA/cm^2, FF of 0.63, and PCE of 4.57%. If the mesoporous TiO_2 layer is thicker than 300 nm, which exceeds the exciton diffusion length of perovskite material, J_{sc} greatly decreases from 11.49 to 1.61 mA/cm^2; however, when the thickness is less than 100 nm, the perovskite layer is discontinuous because the mesoporous TiO_2 layer is too thin to adsorb enough active materials (Figure S2a). In addition, the perovskite layer on the substrate without mesoporous TiO_2 layer presents obvious defects (Figure S2b), resulting in an almost non-functional device. Since the device performance is quite sensitive to mesoporous layer thickness, the optimized thickness was used in the following research. In addition, different kinds of mesoporous layer may improve the devices, such as Al_2O_3 and SrTiOx.[24] More work

is on the way in our lab.

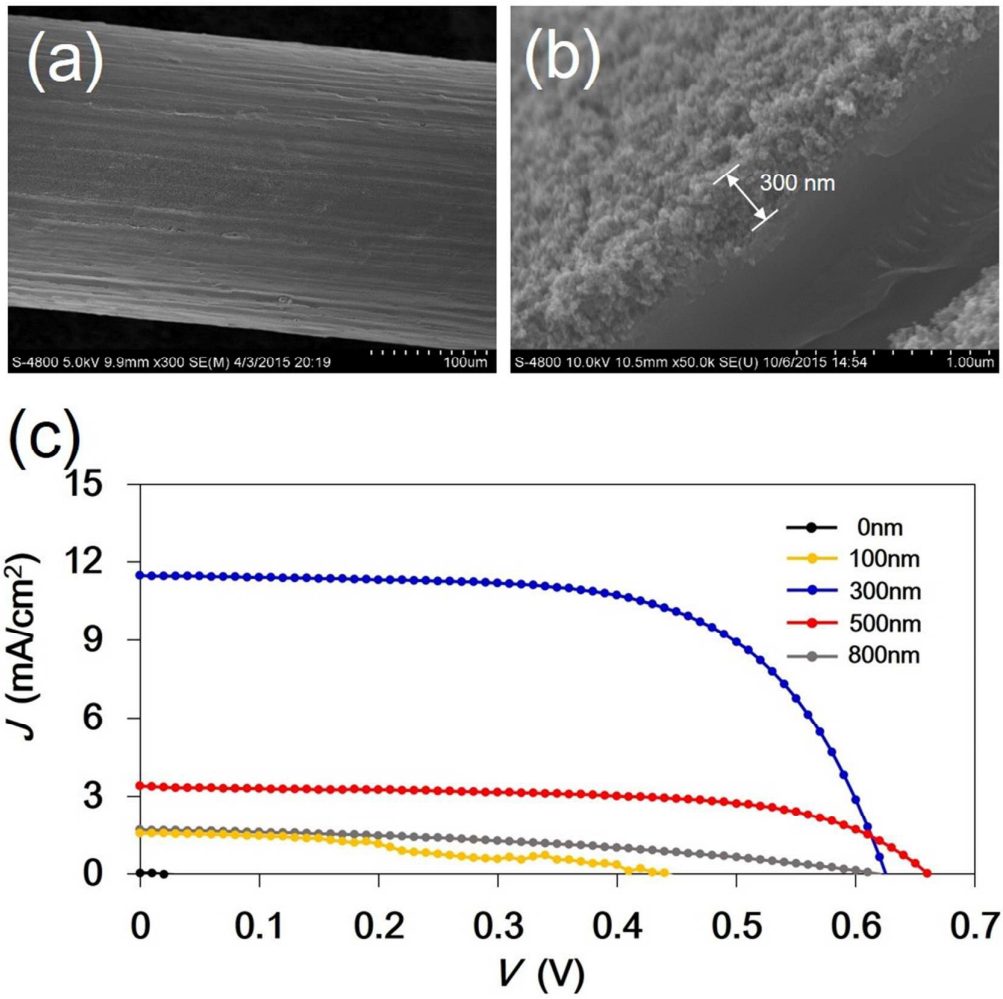

Figure 3. (a) Surface morphology and (b) cross section of 300 nm mesoporous TiO_2 layer. (c) J–V curves of FPSCs with different mesoporous TiO_2 layer thicknesses. (Here, the 0 nm mesoporous TiO_2 layer means the device was not coated with the mesoporous TiO_2 layer).

The morphology of the perovskite layer is also crucial to solar cell performance.[25] We adopted DMF solution of CH_3NH_2I and $PbCl_2$ as precursor because of the one step process is suitable for exploring different coating processes. In the present work, the

morphology of the perovskite film can be regulated by applying different coating processes of dip-coating and infiltration (Figure 4).

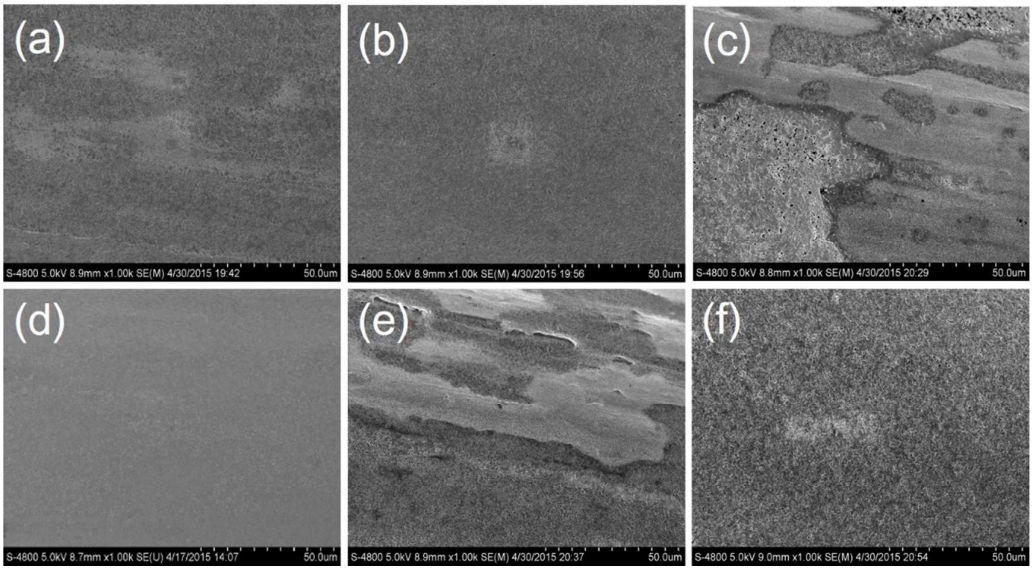

Figure 4. Surface morphology of perovskite film after (a) dip-coating once, (b) dip-coating twice, (c) 2 min of infiltration, (d) 2 min of infiltration then dip-coating, (e) 10 min of infiltration, and (f) 10 min of infiltration then dip-coating.

In Figures 4a–4f, a non-uniform perovskite layer can be deposited after three different coating processes: dip-coating once (Figure 4a), 2 min of infiltration (Figure 4c), and 10 min of infiltration (Figure 4e), and many discrete blocks were formed. We find that a second cycle of dip-coating with the same infiltration duration can induce the perovskite film to become more homogeneous as shown in Figures 4b, 4d, and 4f. Although the surface morphology is similar, different infiltration duration visible impacts on the PCE of the FPSCs (as summarized in Table S1). It will make perovskite precursor solution to infiltrate into the mesoporous TiO_2 layer fully under appropriate infiltration duration. At excessively long infiltration durations, the coating

layer may re-dissolve; by contrast, at short infiltration durations, the perovskite material cannot fully infiltrate into the mesoporous TiO_2 layer. In the experiments, the optimal PCE of FPSCs (V_{oc} of 0.67 V, J_{sc} of 11.23 mA/cm^2, FF of 0.58, and PCE of 4.42%) was observed under 2 min infiltration and dip-coating. As shown in Figure 5, a homogeneous perovskite capping layer is formed, which could inhibit carrier recombination.[26] If the perovskite capping layer is non-uniform, the hole-transport layer perhaps cannot completely cover the perovskite layer and may result in short-circuit. We believe that dip-coating speed and infiltration duration both impact surface morphology by a dynamic process. Also, the thickness of perovskite layer and its influence were studied by adjusting concentration of perovskite precursor solution. The thickness of perovskite layer increased with increasing concentration of perovskite precursor solution. When the concentration increased from 20% to 40%, the PCE of FPSC improved from 0.1% to 4% (Figure S3).

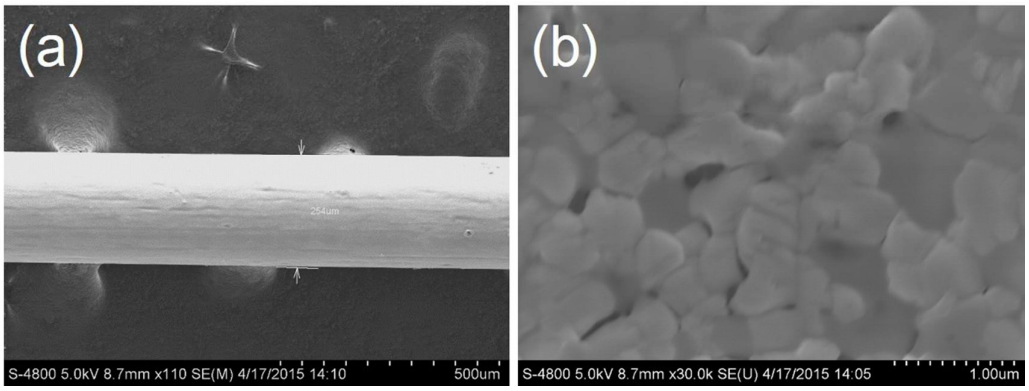

Figure 5. (a) Fiber functional electrode with perovskite layer. (b) Surface morphology of the perovskite capping layer.

Given that the perovskite layer could only harvest light passing through the top

electrode, transparent conductive materials are indispensable for FPSCs. The thin film of gold nanoparticles was prepared via magnetron sputtering[27], which is almost harmless for as-prepared layers, and can easily be industrialized. The transmittance of gold thin film with different sputtering time is provided in Figure S4. Considering that the gold nanoparticles (20–50 nm) were dotted on the sublayer surface (Figures 6a and 6b), the accurate thickness of gold layer could not be determined. We notice that the transmittance and conductivity of the gold thin film can be balanced by varying the sputtering time. The measured relationship between the surface resistance and the transmittance is shown in Figure 7. When magnetron sputtering process durations increases from 10 s to 25 s, the surface resistance of thin film reduced from 72 Ω/cm^2 to 6 Ω/cm^2, while the transmittance of the gold layer decreased from 79% to 64% (at 525 nm) When sputtering gold thin film for 15s, the transmittance is about 76 %, which is enough for solar energy harvesting; and the surface resistance is 12 Ω/cm^2, which is very similar to the surface resistance of commercial FTO glass (~11 Ω/cm^2). Thus, we regard this condition as the best condition to balance transmittance and conductivity for FPSCs.

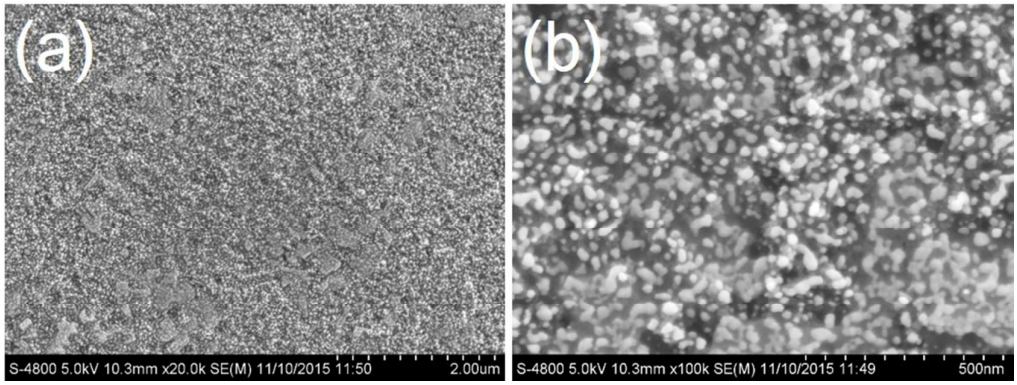

Figure 6. (a) The gold nanoparticles were uniformly distributed on the functional layer.

(b) The gold nanoparticle size was about 20-50 nm.

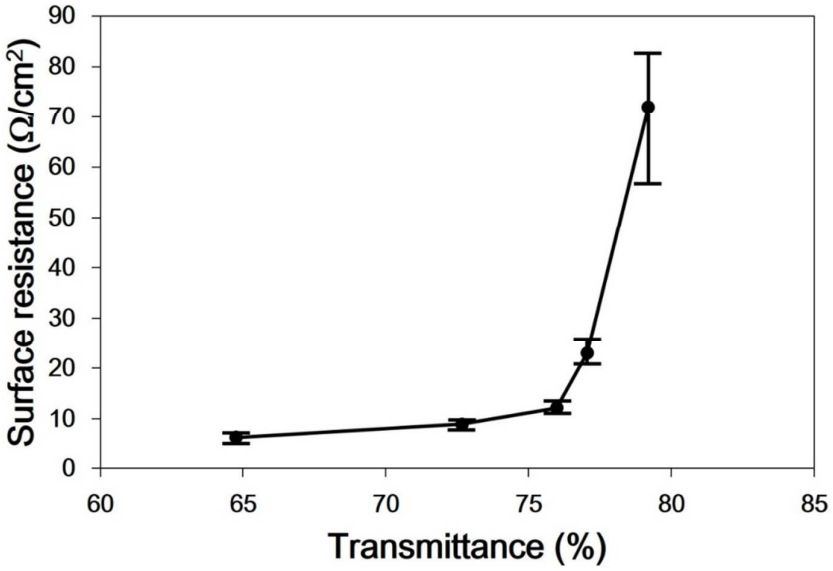

Figure 7. The relation curve between the surface resistance and transmittance of the thin gold electrode at 525 nm.

To ensure accuracy of FPSCs measurement, the above active part that was not twisted with the gold wire but could contribute to photocurrent was cut off. Upon layer-by-layer optimization, the best-performing FPSC achieved a PCE of 5.35% with V_{oc} of 0.714 V, J_{sc} of 12.32 mA/cm^2, FF of 0.609 (Figure 8a), which is currently the highest PCE ever reported for FPSCs. In a series of repeated device preparation, a quarter (25%) of the devices achieved efficiencies >4% (Figure 8b), which are higher than most literature results for solid fiber solar cells. For example, organic fiber solar cells achieved 3.9% PCE in the study of A. Guadiana *et al.*[18], and silicon p-i-n junction fibers obtained 0.5% PCE in the study of V. Badding *et al.*[17] The average efficiency of 40 devices is 3.36%, indicating the high reproducibility of device fabrication in the present period. In addition, we prepared an active length of 2.5 cm

FPSC and exhibits a high fill factor (V_{oc} of 0.633 V, J_{sc} of 10.27 mA/cm^2, FF of 0.70) in our work (Figure S5), which is the highest fill factor ever reported for FPSCs. The high fill factor could be corporately attributed to matched energy level[28], smooth morphology and suitable thickness of each functional layer, and large interfacial contact of the gold nanoparticles as a top electrode in the device. We made a quintessential model planar device for IPCE measurement, which showed an integrated Jsc of 13.42 mA/cm^2 (Figure S6).

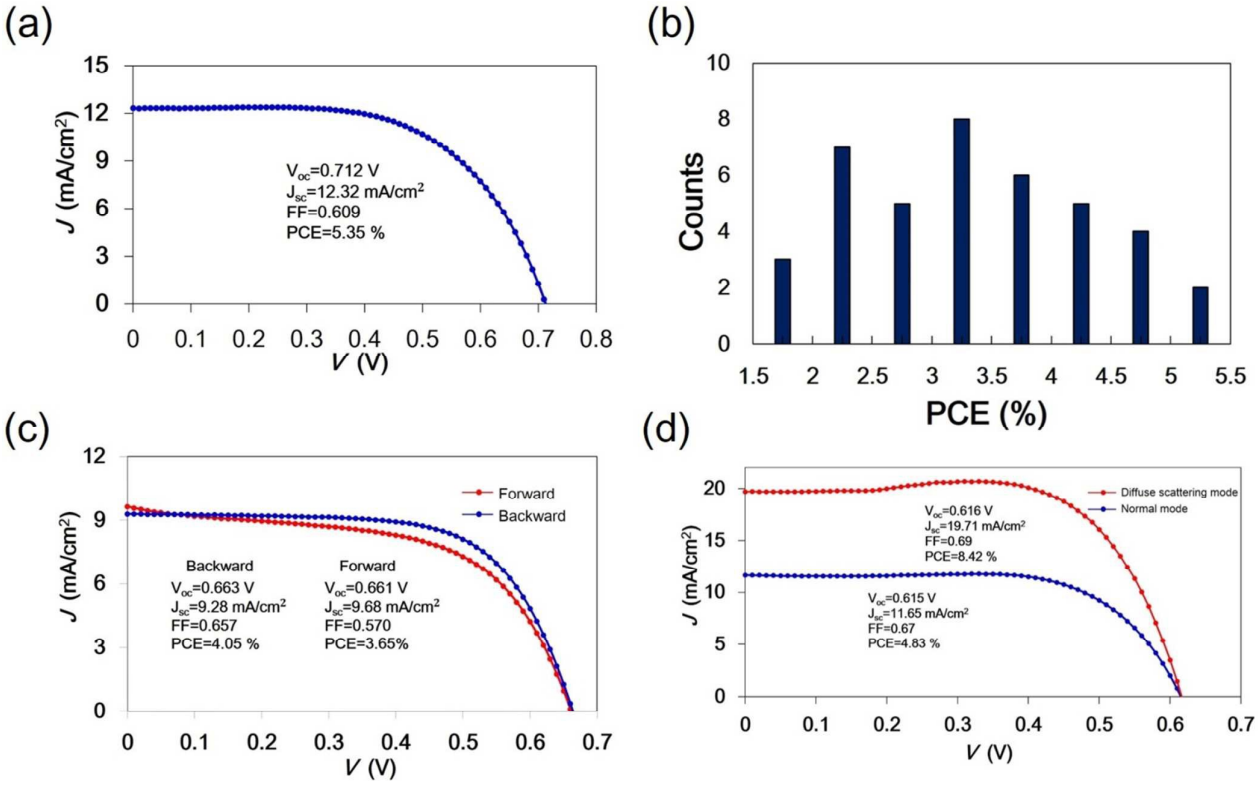

Figure 8. (a) J–V curve of the most efficient FPSCs. (b) Histogram of solar cell efficiencies for 40 devices. (c) J–V curve of the device scanning forward and backward results. (d) J–V curve of diffuse scattering and normal modes.

In this case, forward and backward scan results are barely different. (Figure 8c)

FPSCs feature 3D light harvesting property similar to other fiber-shaped solar cells. The diffused light received by the reflector enhances the apparent efficiency by 174% (from 4.83% to 8.42%), which can enhance power outputs for practical applications (Figure 8d).

Conclusions

In summary, we fabricated fiber-shaped perovskite solar cells with a maximum PCE of 5.35%, which is among the best reported for solid fiber solar cells. $CH_3NH_3PbI_{3-x}Cl_x$ was employed as the functional layer via the simple dip-coating process, and the thin film of gold nanoparticles applied through magnetron sputtering was used as the semitransparent top electrode for the FPSC. Effects of electric heating in situ preparation of compact TiO_2 layer, thickness of TiO_2 porous layer, morphology of perovskite layer were studied. All the preparations are easy to handle and the device reproducibility is promising. The developed solid fiber solar cells may be further developed to wearable devices, such as the strap of a smart watch. Our work may pave the way toward the development of efficient solid fiber solar cells.

Experimental Section

Materials

The Ti wire used was 250 μm in diameter (Alfa Aesar, 99.7%). Commercial TiO_2 nanoparticle paste (Dyesol DSL 18NR-T) was diluted with ethanol (1:7 w/w) and then placed in an ultrasonic bath for 24 h.

Perovskite precursor solution was prepared by dissolving CH_3NH_3I and PbI_2 (molar ratio of 3:1) in DMF with concentration of 40 wt%. A hole transport material solution contain 72.3 mg of Spiro-OMeTAD in 1 mL of chlorobenzene, which was added 17.5 μL of lithium bis(trifluoromethanesulfonyl)imide (Li-TFSI) solution (520 mg Li-TSFI in 1 mL acetonitrile, Sigma-Aldrich, 99.8%) and 28.8 μL of 4-*tert*-butyl pyridine.[29]

Device fabrication

Fiber-shaped perovskite solar cells were fabricated on Ti wires with a diameter of 250 μm. Firstly, the Ti wires were polished by the mechanical method and cleaned sequentially with deionized water, acetone, and ethanol in an ultrasonic bath for 20 min. The compact TiO_2 layer was prepared by electric heating the titanium substrate in the air with current of 1.58 A for 2 minutes. The Ti wire was dip-coated by a dilute commercial TiO_2 nanoparticle colloid solution along with electrical heat at 0.7 A to form the mesoporous TiO_2 layer. The wire was then heated with a current of 1.58 A for 20 min. The as-prepared wire was dip-coated by perovskite precursor solution with given coating process followed by annealing at 100 °C for 60 min in nitrogen. The wire was dip-coated into Spiro-OMeTAD solution for 2 min. Finally, the Ti wires were fixed to a rotating apparatus, and the thin gold electrode was uniformly coated by magnetron sputtering. A gold wire (25 μm in diameter) entwined FPSCs for adjunctively transferring electric current.

Measurements.

Part of the FPSCs without gold wire entwining were cut off to confirm the active area, and the part of device without gold nanoparticles were scraped to expose the Ti wire

as an anode. The self-standing fiber device was measured without any other substrate unless otherwise specified. The J-V curves of the FPSCs were then measured under AM 1.5 illumination (YSS-5A, Yamashita DESO, Japan). The PCE was calculated according to ref. 13.

Film morphology was observed via field emission SEM (S-4800 Hitachi, Japan).

The transmittance of thin gold layer determined via UV-visible meter, and we use the transmittance at 525 nm. [1,30]

The surface resistance determined by resistivity measuring instruments with four-probe array method.

Acknowledgements

This study is jointly supported by National Natural Science Foundation of China (No. 91333107, No. 51573004), Ministry of Science and Technology of China (No. 2011CB933300) and Ministry of Education of China (No. 20120001140010).

References

1. M. M. Lee, J. Teuscher, T. Miyasaka, T. N. Murakami and H. J. Snaith, *Science*, 2012, **338**, 643-647.
2. J. Burschka, N. Pellet, S. J. Moon, R. Humphry-Baker, P. Gao, M. K. Nazeeruddin and M. Gratzel, *Nature*, 2013, **499**, 316-319.
3. C. Wehrenfennig, G. E. Eperon, M. B. Johnston, H. J. Snaith and L. M. Herz, *Advanced Materials*, 2014, **26**, 1584-1589.
4. S. D. Stranks, G. E. Eperon, G. Grancini, C. Menelaou, M. J. P. Alcocer, T. Leijtens, L. M. Herz, A. Petrozza and H. J. Snaith, *Science*, 2013, **342**, 341-344.
5. Dong Shi, V. Adinolfi, R. Comin, M. Yuan, E. Alarousu, A. Buin, Y. Chen, S. Hoogland, A. Rothenberger, K. Katsiev, Y. Losovyj, X. Zhang, P. A. Dowben, O. F. Mohammed, E. H. Sargent and O. M. Bakr, *Science*, 2015, **347**, 519-522.
6. M. I. Saidaminov, A. L. Abdelhady, B. Murali, E. Alarousu, V. M. Burlakov, W.

Peng, I. Dursun, L. Wang, Y. He, G. Maculan, A. Goriely, T. Wu, O. F. Mohammed and O. M. Bakr, *Nature communications*, 2015, **6**, 7586.
7. J. You, Z. Hong, Y. M. Yang, Q. Chen, M. Cai, T.-B. Song, C.-C. Chen, S. Lu, Y. Liu, H. Zhou and Y. Yang, *ACS Nano*, 2014, **8**, 1674-1680.
8. M. Liu, M. B. Johnston and H. J. Snaith, *Nature*, 2013, **501**, 395-398.
9. J. M. Ball, M. M. Lee, A. Hey and H. J. Snaith, *Energy & Environmental Science*, 2013, **6**, 1739-1743.
10. W. S. Yang, J. H. Noh, N. J. Jeon, Y. C. Kim, S. Ryu, J. Seo and S. I. Seok, *Science*, 2015, **12**, 1-8.
11. H. J. Snaith, *The Journal of Physical Chemistry Letters*, 2013, **4**, 3623-3630.
12. M. A. Green, A. Ho-Baillie and H. J. Snaith, *Nature Photonics*, 2014, **8**, 506-514.
13. M. Peng and D. Zou, *Journal of Materials Chemistry A*, 2015, **3**, 20435-20458.
14. W. Zeng, L. Shu, Q. Li, S. Chen, F. Wang and X. M. Tao, *Adv Mater*, 2014, **26**, 5310-5336.
15. Y. Fu, Z. Lv, S. Hou, H. Wu, D. Wang, C. Zhang and D. Zou, *Advanced Energy Materials*, 2012, **2**, 37-41.
16. G. Liu, M. Peng, W. Song, H. Wang and D. Zou, *Nano Energy*, 2015, **11**, 341-347.
17. R. He, T. D. Day, M. Krishnamurthi, J. R. Sparks, P. J. Sazio, V. Gopalan and J. V. Badding, *Adv Mater*, 2013, **25**, 1461-1467.
18. M. R. Lee, R. D. Eckert, K. Forberich, G. Dennler, C. J. Brabec and R. A. Gaudiana, *Science*, 2009, **324**, 232-235.
19. D. Wang, S. Hou, H. Wu, C. Zhang, Z. Chu and D. Zou, *Journal of Materials Chemistry*, 2011, **21**, 6383-6388.
20. L. Qiu, J. Deng, X. Lu, Z. Yang and H. Peng, *Angew Chem Int Ed Engl*, 2014, **53**, 10425-10428.
21. M. Lee, Y. Ko and Y. Jun, *Journal of Materials Chemistry A*, 2015, **3**, 19310-19313.
22. J. H. Yum, P. Chen, M. Gratzel and M. K. Nazeeruddin, *ChemSusChem*, 2008, **1**, 699-707.
23. A. Abrusci, S. D. Stranks, P. Docampo, H. L. Yip, A. K. Jen and H. J. Snaith, *Nano letters*, 2013, **13**, 3124-3128.
24. A. Bera, K. Wu, A. Sheikh, E. Alarousu, O. F. Mohammed and T. Wu, *The Journal of Physical Chemistry C*, 2014, **118**, 28494-28501.
25. G. E. Eperon, V. M. Burlakov, P. Docampo, A. Goriely and H. J. Snaith, *Advanced Functional Materials*, 2014, **24**, 151-157.
26. N. Li, H. Dong, H. Dong, J. Li, W. Li, G. Niu, X. Guo, Z. Wub and L. Wang, *Journal of Materials Chemistry A*, 2014, **2**, 14973-14978.
27. K. Fuchs, *Proceedings of the Cambridge Philosophical Society*, 1938, **34**, 100-108.
28. L. Lu, T. Xu, I. H. Jung and L. Yu, *The Journal of Physical Chemistry C*, 2014, **118**, 22834-22839.

29. J.-H. Im, I.-H. Jang, N. Pellet, M. Grätzel and N.-G. Park, *Nature Nanotechnology*, 2014, **9**, 927-932.
30. H. Zhou, Q. Chen, G. Li, S. Luo, T. B. Song, H. S. Duan, Z. Hong, J. You, Y. Liu and Y. Yang, *Science*, 2014, **345**, 542-546.

Table of Contents

The fiber-shaped perovskite solar cells achieved a PCE of 5.3% based on the structure of Ti/ c-TiO_2/meso-TiO_2/perovskite/Spiro-OMeTAD/Au.